

# Charge density waves and electronic properties of superconducting kagome metals

Hengxin Tan,<sup>1</sup> Yizhou Liu,<sup>1</sup> Ziqiang Wang,<sup>2</sup> and Binghai Yan<sup>1</sup>

<sup>1</sup>*Department of Condensed Matter Physics, Weizmann Institute of Science, Rehovot 7610001, Israel*

<sup>2</sup>*Department of Physics, Boston College, Chestnut Hill, Massachusetts 02467, USA*

(Dated: February 28, 2025)

Kagome metals  $AV_3Sb_5$  ( $A = K, Rb, \text{ and } Cs$ ) exhibit intriguing superconductivity below  $0.9 \sim 2.5$  K with possibly  $\mathbb{Z}_2$  topological surface states, after a charge density wave (CDW) transition around  $80 \sim 100$  K. The nature of the CDW phase and its relation to the superconductivity remain elusive. In this work, we investigate the electronic and structural properties of the CDW phase by first-principles simulations. We reveal an *inverse* star of David structure as the  $2 \times 2$  CDW ground state of the kagome lattice. The CDW transition is driven by the Peierls instability characterized by the softening of a breathing phonon mode in the kagome lattice. The simulated scanning tunneling microscopy (STM) images of the inverse star of David structure agree with recent experiments on the  $KV_3Sb_5$  surface. The nontrivial  $\mathbb{Z}_2$ -type topological band structure remains the same after the CDW transition. Further, we evaluate the electron-phonon coupling in the CDW phase and find it is too weak to rationalize the superconductivity in all three materials. It implies the existence of unconventional pairing of these kagome metals. Our results provide essential knowledge toward understanding the superconductivity and topology in kagome metals.

## I. INTRODUCTION

The kagome lattice constitutes uniformly tiled triangles and hexagons in a plane. Related insulating materials are actively studied for intriguing phenomena like spin liquids[1], geometrical frustration[2], charge density waves (CDW)[3], and unconventional superconductivity of doped Mott insulators[4]. For the more recent interest of topology, several magnetic kagome metals were found to be magnetic Weyl semimetals[5–7] and exhibit a large anomalous Hall effect[8–11]. Very recently, nonmagnetic kagome metals  $AV_3Sb_5$  ( $A = K, Rb, \text{ and } Cs$ )[12] were reported to exhibit both charge density waves and superconductivity, and  $\mathbb{Z}_2$ -type nontrivial band topology[13, 14], which sparked immediate interest in these materials[15–17].

The pristine phases of  $AV_3Sb_5$  exhibit a uniform kagome lattice of V atoms at room temperature. The  $\mathbb{Z}_2$  topological metal was found by calculations and angle-resolved photoemission spectroscopy[13]. As cooling down to about  $80 \sim 100$  K,  $AV_3Sb_5$  goes through a CDW transition in experiment. The superconductivity emerges from the CDW phase with  $T_c = 0.9 \sim 2.5$  K (see Table I for summary). For  $CsV_3Sb_5$ , very recent experiments reveal possible nodal superconductivity[18] and the competition between superconductivity and CDW[19]. For the CDW phase, X-ray diffraction[13, 14] and scanning tunneling microscopy (STM)[20–23] revealed the formation of a  $2 \times 2$  superlattice, for which Refs.20–22 assumed a Star of David (SD) distortion in the kagome plane and the proximity of the Fermi surface to the van Hove singularity. However, solid knowledge on the lattice and electronic properties for the origin of the CDW state are missing in order to the understand of the superconductivity and topology.

In this work, we have investigated the structural and electronic properties of the CDW phase by first principles calculations. We find that the CDW transition is driven by a breathing phonon mode of the kagome lattice. The resultant  $2 \times 2$  superlattice energetically favors an *inverse*

Star of David (ISD) pattern rather than the SD, for all three compounds. The STM images simulated for the ISD phase agree with the recent experiment. The CDW distortion modulates the Fermi surface but preserves the  $\mathbb{Z}_2$  topology of the pristine phase. We evaluate the electron-phonon coupling in the CDW phase and find it is too weak to interpret the superconductivity in all three materials. It may imply the existence of unconventional superconductivity pairing.

## II. METHODS

Density Functional Theory calculations are performed within the Perdew-Burke-Ernzerhof-type generalized gradient approximation [24], which is implemented in the Vienna *ab-initio* Simulation Package (VASP) [25, 26]. The projected augmented wave [27] potentials with nine valence electrons for the  $A$  atom. The cutoff energy for the plane wave basis set is 300 eV. The zero damping DFT-D3 van der Waals correction [28] is employed throughout the calculations. Spin-orbital coupling (SOC) is considered in the electronic structure calculations but not for the structural relaxation, phonon dispersion and STM simulation. The phonon dispersion is calculated by using the finite displacement method as implemented in the phonopy code [29]. The superconducting temperatures  $T_c$  are estimated under the electron-phonon coupling scenario, where the deformation potential and the electron-phonon coupling constants are estimated by the frozen phonon scheme.

## III. RESULTS

### A. Charge density waves

The pristine phase of  $AV_3Sb_5$  crystallizes in the hexagonal structure with the space group of  $P6/mmm$  (No.191),

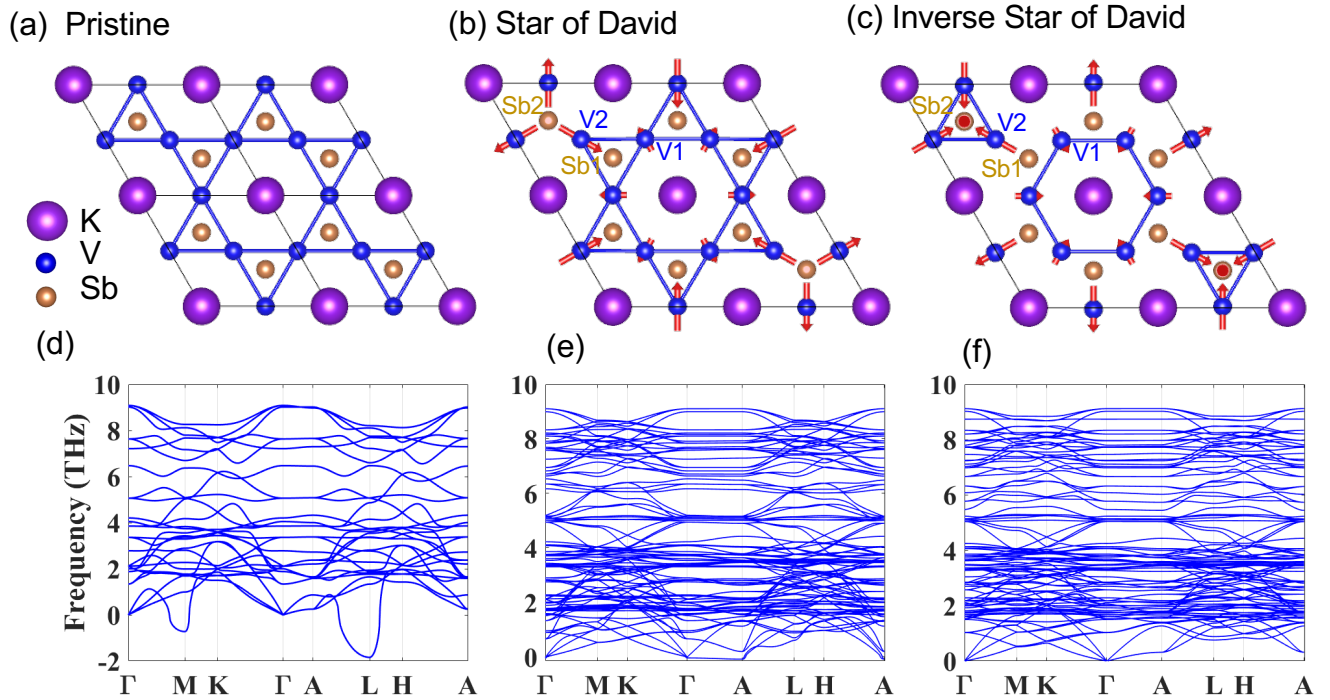


Figure 1. Crystal structures of  $KV_3Sb_5$  in the pristine phase, the Star of David  $2 \times 2$  CDW phase, and the inverse Star of David phase. Corresponding phonon dispersions are shown in the lower panels. A  $2 \times 2$  supercell is shown in (a). Imaginary (negative) phonon frequency in (d) corresponds to the breathing mode of the kagome lattice. Such a breathing-instability leads to CDW distortions. The breathing-out and breathing-in lead to two different structures in (b) and (c), where the red arrows indicate the lattice distortion due to the breathing mode. In CDW phases, V1 and V2 represent inequivalent vanadium sites of the kagome lattice, and Sb1 and Sb2 are inequivalent sites of the honeycomb lattice.

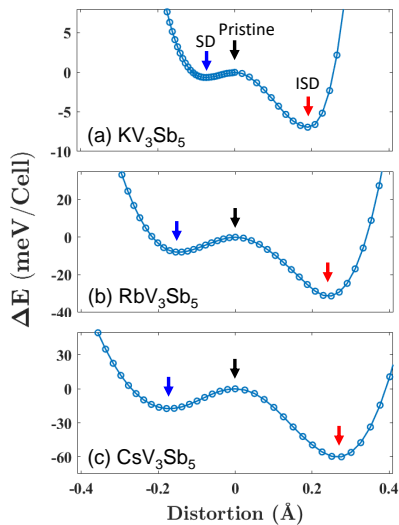


Figure 2. Total energy profiles for the pristine phase, Star of David (SD) and inverse Star of David (ISD) phases. The distortion stands for the amplitude of the breathing phonon mode where the negative values are used for SD in order to distinguish from ISD. The vertical axis stands for the total energy per supercell (36 atoms). Spin-orbit coupling is considered.

as shown in Fig. 1(a). The calculated lattice constants are  $5.41 \text{ \AA}$  (a) and  $8.89 \text{ \AA}$  (c) for  $KV_3Sb_5$ ,  $5.42 \text{ \AA}$  and  $9.09 \text{ \AA}$  for  $RbV_3Sb_5$  and  $5.44 \text{ \AA}$  and  $9.33 \text{ \AA}$  for  $CsV_3Sb_5$ . Within this phase, there are four independent Wyckoff sites:  $(0, 0, 0)$  for alkali atom,  $(0.5, 0, 0.5)$  for V,  $(0, 0, 0.5)$  for Sb1 and  $(1/3, 2/3, z)$  for Sb2, where  $z = 0.7566$  for K,  $0.7501$  for Rb and  $0.7425$  for Cs. The V atoms form the kagome layer and Sb1 occupies the centers of the V hexagons. This kagome layer is sandwiched by the honeycomb lattices of Sb2. Neighboring kagome layers are separated by alkali ions. Three materials are nonmagnetic in our calculations, consistent with experiments[12, 30].

The pristine phases exhibit a structural instability. Let's take  $KV_3Sb_5$  as an example. Its phonon band structure in Fig. 1(d) shows a softening acoustic phonon modes at the Brillouin Zone boundary near  $M$  and  $L$  points, indicating the strong instability. Extended to the  $2 \times 2$  supercell, the soft mode corresponds to a breathing phonon ( $A_{1g}$  symmetry) of V atoms in the kagome lattice [Figs. 1(b) and (c)]. Breathing-in and out lead to two different structures. The SD structure forms when V1 (V2) atoms moves away (toward to) the center, which is similar to the known CDW of  $1T \text{ TaS}_2$ [31], while the ISD structure forms by an inverse deformation to the SD. Both SD and ISD exhibit an in-plane  $2 \times 2$  modulation of the structure. The  $2 \times 2$  superlattice have the same

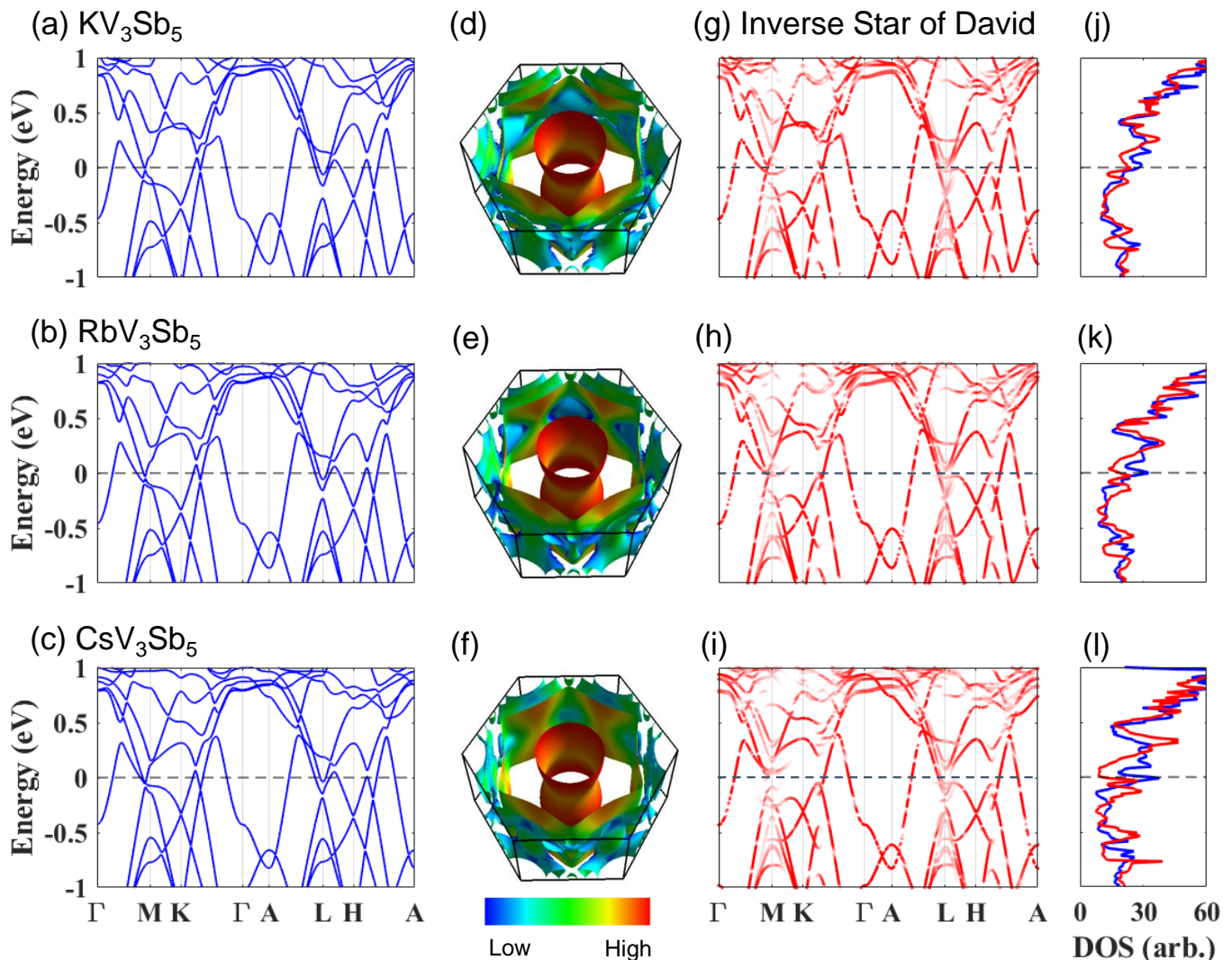


Figure 3. Electronic structures. (a-c) show the band structure for the pristine phase. (d-f) show the Fermi surface for the pristine phase, where the color stands for the Fermi velocity. (g-i) show the unfolded band structure of the inverse Star of David phase. (j-l) show the total DOS of the pristine (blue) and inverse Star of David (red) phases. The red color represents the  $1 \times 1$  spectrum weights. Spin-orbit coupling is included.

space group of  $P6/mmm$  as the pristine phase but two inequivalent sites (V1 and V2).

For all three compounds, the optimized SD and ISD structures are locally stable. The imaginary frequencies disappear in their phonon spectra except a faint soft feature in the SD case (see more details in the Supplementary Material (SM)[32]). We find that the SD phase is higher in energy than the ISD phase for all the three materials. As shown in Fig. 2, the ISD phase is more and more energetically favored from K, to Rb and Cs. Besides, the distortion also becomes larger from K, to Rb and Cs. Therefore, the ISD is more likely the ground state structure, compared to the SD, in the  $2 \times 2$  CDW phase. This observation will be verified by the STM images in Section III C.

The CDW is induced by the Peierls instability related

to the Fermi surface nesting and phonon softening[33, 34]. The  $q$  vector of the soft phonon at  $M$  coincides with the Fermi nesting vector between neighboring van Hove singularities in the Fermi surface of  $AV_3Sb_5$  (see Fig.3). As a consequence, the CDW deformation strongly reduces the density of states (DOS) at the Fermi energy by suppressing the van Hove singularities. Related Fermi surface nesting, CDW and their competition with superconductivity are extensively discussed for the kagome lattice model in literature[35–38].

Above energetics and structures of two CDW phases are studied for bulk materials. When forming a surface with different charging or atomic-terminations, the ISD or SD structure may deviate on the surface. To examine the CDW stability on the surface, we have performed surface calculations using a slab model that is

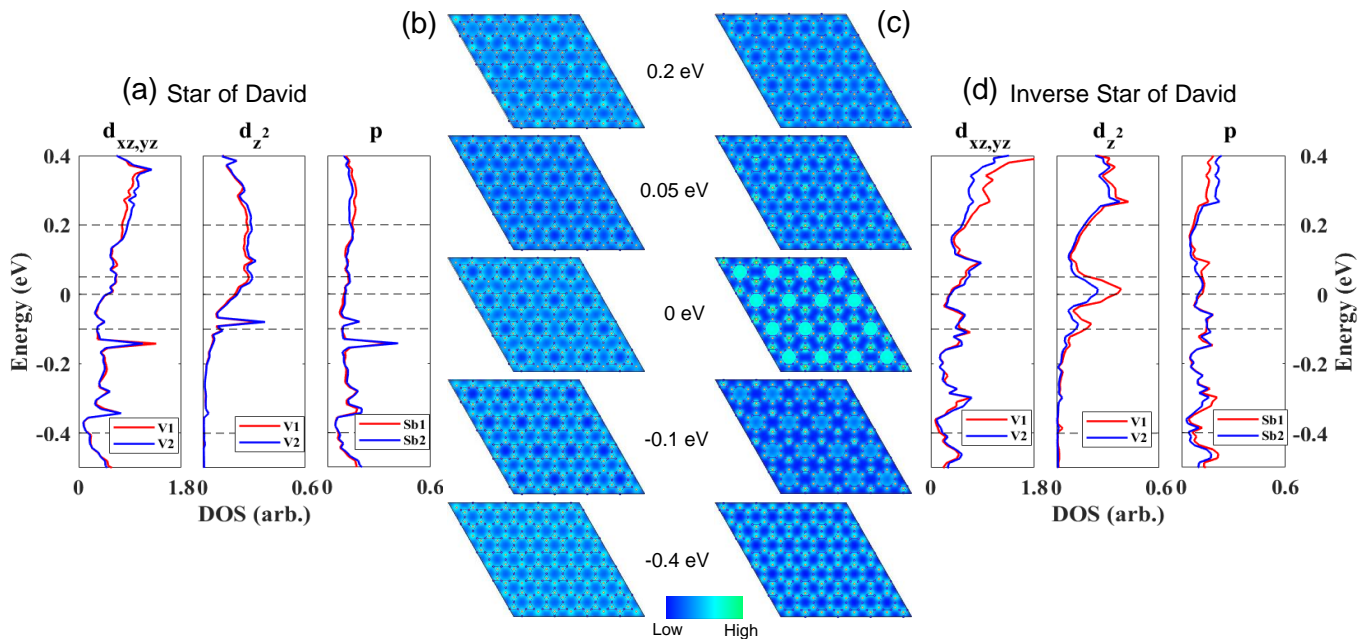


Figure 4. Surface orbital-resolved DOS and simulated STM images for the  $2 \times 2$  CDW phases of  $KV_3Sb_5$ : (a) and (b) for the Star of David structure, (c) and (d) for the inverse Star of David structure. The V1, V2, Sb1 and Sb2 in (a) and (d) are labeled in Fig. 1 (b) and (c). The DOS of V- $d$  and Sb- $p$  states are projected. The V1, V2, Sb1 and Sb2 are superposed on the images for reference.

four-unitcell thick. Recent experiments[20, 21, 23] observed both  $A$  and Sb terminations on cleavage surfaces. We find that the ISD phase is still as stable as the bulk phase for the  $A$ -termination. However, the ISD deformation tends to be weaker (closer to the pristine case) on the Sb-terminated surface than in the bulk. The SD phase exhibits a similar trend. But the ISD structure is still more energetically favored than the SD one. The surface atomic relaxation indicates the instability of the  $2 \times 2$  CDW on the Sb-terminated surface. We note that recent experiments[21, 23] reveals the existence of a  $4 \times 1$  pattern when cooling down further after the  $2 \times 2$  CDW transition. The emerging  $4 \times 1$  pattern may be due to electron correlations related to above surface instability and electron-phonon interaction.

Further, the very recent STM measurement[22] revealed a three-dimensional CDW, i.e., the  $2 \times 2 \times 2$  CDW, for  $CsV_3Sb_5$ . This coincides with the inter-layer instability characterized by the soft phonon mode at the  $L$  (0.5 0.5 0.5) point in the phonon spectrum [Fig.1(d)]. Our calculations confirm that the  $\pi$  CDW-phase-shift between neighboring layers reduces slightly the binding energy by  $\sim 10$  meV per  $2 \times 2$  layer for  $CsV_3Sb_5$ . In the  $2 \times 2 \times 2$  CDW, the SD phase is no longer meta-stable and relaxes to the ISD phase spontaneously. Therefore, the ISD deformation is still preferred in energy. Additionally, the  $2 \times 2 \times 2$  CDW exhibits nearly the same electronic structure as the  $2 \times 2 \times 1$  one, because of the weak inter-layer interaction. For simple, we focus on the  $2 \times 2 \times 1$  (i.e.,  $2 \times 2$ ) CDW phase in the following discussions.

## B. Band structures

The band structures of the pristine phase are shown in Fig. 3(a)-(c) for three materials, which are similar to the previous report. We should note that the Fermi energy (charge neutral point) in our work is about 0.1 eV higher than that of Ref.[12]. Such a minor derivation lifts the Fermi energy above the van Hove singularity point at  $M$  and leads to a slightly different Fermi surface (FS) near the Brillouin zone boundary [Fig. 3(d)-(f)]. The FSs exhibit a strong 2D feature, which is characterized by the cylinder-like FS (Sb- $p$  states) centered around  $\Gamma$ , and the large hexagonal FS (V- $d$  states). There are also much smaller FSs (V- $d$  states) near  $M/L$  and  $K/H$ . Additionally, one can also observe the 2D feature in the weak  $\Gamma - A$  dispersion in the phonon spectrum [Fig.1(d)].

The  $2 \times 2$  ISD CDW distortion modifies the FSs. We unfold the band structure of the ISD phase to the pristine Brillouin zone in Figs. 3(g)-(i). These bands near the Brillouin zone boundary (e.g.,  $M$  and  $K$ ) are strongly modified, including the large hexagonal FS and small FSs, although the cylinder-like FS is nearly unchanged. It is not surprising that the breathing distortion changes mainly the V- $d$  driven states. The van Hove singularities slightly below the Fermi energy at  $M$  are strongly suppressed by the CDW distortion. Consequently, CDW reduces the total density of states (DOS) near the Fermi energy [Fig. 3(j)-(l)], which is also consistent with recent STM spectra[20, 22, 23]. The Cs compound exhibits stronger modifications in FSs and DOS than the K and Rb compounds. This is mainly because the V atom displacement

becomes larger from K, to Rb and Cs compounds (see Fig.2).

The band structure of the pristine phase was reported to exhibit nontrivial band inversion [13, 14]. For the CDW phases, we calculate the  $\mathbb{Z}_2$  topological invariants by the parity eigenvalues [39]. We find that both SD and ISD phases are still  $\mathbb{Z}_2$  nontrivial topological metals (see SM[32] for details).

### C. STM images

The existence of SD/ISD CDW can be examined via the STM images in experiments. Therefore, we have simulated STM images for two CDW phases for all three materials. We also take the K compound for example here. We calculate the local density of states (LDOS) in the plane that is  $\sim 3 \text{ \AA}$  above the Sb-terminated surface (in a slab model[32]), to simulate the STM dI/dV mapping. For a given bias  $V_b$ , the LDOS is summed in the energy range of  $V_b \pm 25 \text{ meV}$ . Figures 4(a)&(d) show the surface DOS contributed by V1, V2, Sb1 and Sb2 atoms [labeled in Fig. 1(b) and (c)], which rationalizes the differences of STM images between SD and ISD phases

The most characteristic feature near the Fermi energy is that the ISD structure exhibits a large, bright  $2 \times 2$  spots by the V1-hexagon centers while the SD structure exhibits bright circles around the V1-hexagon with the hexagon center being dark. The V1-hexagon centers turn quickly dark as moving away from the zero energy, which agrees with recent STM results for  $\text{KV}_3\text{Sb}_5$  in Ref.[20]. Also supported by the lower total energy, we conclude that the ground state of the  $2 \times 2$  CDW phase exhibits more likely the ISD structure for these three compounds. The high LDOS at V1-hexagon centers is caused by the large peak of V1- $d_{z^2}$  and small V1- $d_{xz,yz}$  in DOS [Fig.4(d)]. In contrast, no such a peak appears for the V1- $d_{z^2}$  on SD surface [Fig.4(a)].

At  $V_b = 0.05 \text{ eV}$ , the V1-hexagon brightness greatly decreases due to the decreasing DOS of V- $d_{z^2}$  on the ISD surface. At the same time, the V- $d_{xz,yz}$  DOS increases, where the V2- $d_{xz,yz}$  contribution is slightly larger than the V1- $d_{xz,yz}$  one. Thus, small V2-triangles turn brighter. For the SD surface, the STM image at  $V_b = 0.05 \text{ eV}$  remains almost the same as that at zero, because the relative amplitudes of DOS between V1 and V2 are nearly unchanged. For  $V_b = 0.2 \text{ eV}$ , the ISD surface exhibits bright circles, because V1 is larger in DOS than V2. In contrast, the SD surface shows small, bright spots at V2-triangles, caused by the relative larger DOS of V2 than that of V1.

At  $V_b = -0.1 \text{ eV}$ , the ISD surface looks less-contrast in the STM image compared to the zero bias case, due to the decreasing V- $d_{z^2}$  and increasing V- $d_{xz,yz}$  in DOS. For the SD surface, all the atomic sites show similar brightness due to the small DOS peaks of V- $d$  and Sb- $p$  near  $-0.1 \text{ eV}$ . At  $V_b = -0.4 \text{ eV}$ , both ISD and SD surfaces show a  $1 \times 1$  honeycomb pattern. The honeycomb feature reflects

the top Sb layer (Sb1 and Sb2), although V is comparable to Sb in DOS.

We note that STM images of  $\text{RbV}_3\text{Sb}_5$  and  $\text{CsV}_3\text{Sb}_5$  (see SM [32]) share similar features as those of  $\text{KV}_3\text{Sb}_5$ .

### D. Superconductivity

$\text{AV}_3\text{Sb}_5$  exhibits superconductivity from the CDW normal state. The most recent STM experiment [23] on  $\text{CsV}_3\text{Sb}_5$  reveals a superconducting gap  $\sim 0.5 \text{ meV}$ , which puts the superconductor in the strong-coupling regime with  $2\Delta/k_B T_c$  around 4.6. A natural question is whether the superconductivity is driven by the electron-phonon coupling in Bardeen-Cooper-Schrieffer (BCS) scenario [40]. Therefore, we have calculated the electron-phonon coupling constant ( $\lambda$ ) for the ISD phase and estimated the  $T_c$  based on McMillan's formula which applies in the strong-coupled regime [41],

$$T_c = \frac{\theta_D}{1.45} \exp \left[ -\frac{1.04(1+\lambda)}{\lambda - \mu^*(1+0.62\lambda)} \right], \quad (1)$$

with  $\theta_D$  being the Debye temperature which can be extracted through a quadratic fitting of the phonon density of states of the low frequency acoustic bands:  $g(\omega) = \alpha\omega^2$ . Using the fitted value of  $\alpha$ , the Debye temperature is determined by  $\theta_D = (\hbar/k_B)(9N/\alpha)^{1/3}$  where  $N$  and  $k_B$  are the total number of atoms within a unit cell and the Boltzmann constant, respectively. This relation is determined by the total number of phonon modes  $3N = \int_0^{\omega_D} g(\omega) d\omega$  where  $\omega_D = k_B\theta_D/\hbar$  is the Debye angular frequency.

$\lambda$  ( $\mu^*$ ) is a dimensionless parameter describing the strength of effective electron-electron attractive (screened-repulsive) interaction [42] and the superconductivity can happen only when  $\lambda > \mu^*$ . The value of  $\mu^*$  is assumed in the range 0.10–0.15 [43, 44]. And  $\lambda$  is calculated based on deformation potential approximation [43, 45],

$$\begin{aligned} \lambda &= N_F \langle V_{\text{ph}} \rangle_{E_F} = N_F \sum_{\omega} \left\langle \frac{|\mathcal{M}_{\text{e-ph}}|^2}{\hbar\omega} \right\rangle_{E_F} \\ &= N_F \sum_{\omega} \frac{|D|^2}{2M\omega^2} \end{aligned} \quad (2)$$

where  $N_F$  is the electron DOS per spin per unit cell,  $V_{\text{ph}}$  is the phonon-mediated effective electron-electron interaction energy,  $\mathcal{M}_{\text{e-ph}}$  is the electron-phonon matrix element,  $\omega$  is the phonon frequency,  $M$  is atomic mass, and  $D$  is the electronic deformation potential.  $\langle \rangle_{E_F}$  refers to the averaging at Fermi energy  $E_F$ . According to Eq. (2) phonon modes with lower frequency and stronger deformation potential contributes most to  $\lambda$ . We approximate  $\lambda$  by considering only the breathing mode and the deformation potential  $D \approx \Delta E_k / \Delta u_{\text{breathing}}$  with  $\Delta E_k$  being the average shift of band energy at Fermi energy and  $\Delta u_{\text{breathing}}$  is the deformation amplitude. We further simplify the expression of  $\lambda$  by  $M\omega_{\text{breathing}}^2 = \langle \Phi \rangle_{\text{breathing}}$  with  $\langle \Phi \rangle_{\text{breathing}}$  being the average force constant of the

Table I. Estimation of the  $T_c$  due to electron-phonon coupling. We list the CDW transition temperature  $T_{\text{CDW}}^{\text{exp.}}$ , experimental superconducting temperature  $T_c^{\text{exp.}}$  and experimental Debye temperature  $\theta_D^{\text{exp.}}$  in unit of K [13, 14, 46]. We show calculation parameters and results: DOS per superlattice at the Fermi energy  $N_F$  ( $\text{eV}^{-1}$ ), deformation potential  $D$  ( $\text{eV}/\text{\AA}$ ), phonon mediated electron-electron attractive interaction strength  $\lambda$ , calculated Debye temperature  $\theta_D$ , and calculated  $T_c$  for the ISD phase.

	$T_{\text{CDW}}^{\text{exp.}}$	$N_F$	$D$	$\lambda$	$\theta_D$	$\theta_D^{\text{exp.}}$	$T_c$	$T_c^{\text{exp.}}$
KV <sub>3</sub> Sb <sub>5</sub>	78	11.6	0.52	0.46	158	68	0.38–1.13	0.93
RbV <sub>3</sub> Sb <sub>5</sub>	102	9.3	0.56	0.39	191	169	0.10–0.54	0.92
CsV <sub>3</sub> Sb <sub>5</sub>	94	5.2	0.76	0.30	121	–	0.0017–0.055	2.5

breathing mode. More details of the calculation of  $\lambda$  and  $\theta_D$  are shown in SM [32].

Table I lists the calculated parameters  $N_F$ ,  $D$ ,  $\lambda$ ,  $\theta_D$ , and  $T_c$  for ISD phase of three materials. The  $D$  values are one order of magnitude smaller than the known BCS superconductor MgB<sub>2</sub> [43] but the  $\lambda$  fall into a moderate region as compensated by large  $N_F$ . All the  $\lambda$  are smaller than 1, indicating that they are in the weakly-coupled regime. The calculated  $\theta_D$  is larger than experimental values for RbV<sub>3</sub>Sb<sub>5</sub> [46] and KV<sub>3</sub>Sb<sub>5</sub> [14]. The smallness of  $\lambda$  of CsV<sub>3</sub>Sb<sub>5</sub> is mainly due to the low DOS at the Fermi energy. The upper limit of calculated  $T_c$ , which is already overestimated due to  $\theta_D$ , is much smaller than corresponding experimental value. This indicates the unconventional mechanism of the superconductivity observed in these

materials.

#### IV. SUMMARY

In summary, we have studied the crystal and electronic structures of the CDW phases of three kagome metals AV<sub>3</sub>Sb<sub>5</sub>. The 2×2 CDW (also the 2 × 2 × 2 one) phase exhibits an inverse Star of David deformation. Corresponding STM images simulated agree with recent experiments. The nontrivial  $\mathbb{Z}_2$  nature remains in the CDW band structure. We have evaluated the superconducting temperature induced by electron-phonon coupling and found it is much smaller than corresponding experimental value, implying possible unconventional superconductivity in these materials.

#### V. ACKNOWLEDGEMENTS

We thank H. Chen for inspiring discussions and A. Perara for help in calculations. B.Y. acknowledges the financial support by the Willner Family Leadership Institute for the Weizmann Institute of Science, the Benozio Endowment Fund for the Advancement of Science, Ruth and Herman Albert Scholars Program for New Scientists, the European Research Council (ERC) under the European Union’s Horizon 2020 research and innovation programme (Grant No. 815869). Z.W. is supported by the U.S. Department of Energy, Basic Energy Sciences Grant No.DE-FG02-99ER45747.

- 
- [1] Matthew P Shores, Emily A Nytko, Bart M Bartlett, and Daniel G Nocera, “A structurally perfect  $s=1/2$  kagome antiferromagnet,” *Journal of the american chemical society* **127**, 13462–13463 (2005).
- [2] A P Ramirez, “Strongly geometrically frustrated magnets,” *Annual Review of Materials Science* **24**, 453–480 (1994).
- [3] S. V. Isakov, S. Wessel, R. G. Melko, K. Sengupta, and Yong Baek Kim, “Hard-Core Bosons on the Kagome Lattice: Valence-Bond Solids and Their Quantum Melting,” *Physical Review Letters* **97**, 147202 (2006).
- [4] Wing-Ho Ko, Patrick A. Lee, and Xiao-Gang Wen, “Doped kagome system as exotic superconductor,” *Physical Review B* **79**, 214502 (2009).
- [5] Hao Yang, Yan Sun, Yang Zhang, Wu-Jun Shi, Stuart S P Parkin, and Binghai Yan, “Topological Weyl semimetals in the chiral antiferromagnetic materials Mn<sub>3</sub>Ge and Mn<sub>3</sub>Sn,” *New Journal of Physics* **19**, 015008 (2017).
- [6] Noam Morali, Rajib Batabyal, Pranab Kumar Nag, Enke Liu, Qiunan Xu, Yan Sun, Binghai Yan, Claudia Felser, Nurit Avraham, and Haim Beidenkopf, “Fermi-arc diversity on surface terminations of the magnetic weyl semimetal  $\text{Co}_3\text{Sn}_2\text{S}_2$ ,” *Science* **365**, 1286–1291 (2019).
- [7] DF Liu, AJ Liang, EK Liu, QN Xu, YW Li, C Chen, D Pei, WJ Shi, SK Mo, P Dudin, *et al.*, “Magnetic weyl semimetal phase in a kagomé crystal,” *Science* **365**, 1282–1285 (2019).
- [8] Satoru Nakatsuji, Naoki Kiyohara, and Tomoya Higo, “Large anomalous Hall effect in a non-collinear antiferromagnet at room temperature,” *Nature* **527**, 212 – 215 (2015).
- [9] A K Nayak, J E Fischer, Y. Sun, B Yan, J Karel, A C Komarek, C Shekhar, N Kumar, W Schnelle, J Kuebler, C. Felser, and S.S.P. Parkin, “Large anomalous Hall effect driven by a nonvanishing Berry curvature in the noncollinear antiferromagnet Mn<sub>3</sub>Ge,” *Science Advances* **2**, e1501870 – e1501870 (2016).
- [10] Enke Liu, Yan Sun, Nitesh Kumar, Lukas Muechler, Aili Sun, Lin Jiao, Shuo-Ying Yang, Defa Liu, Aiji Liang, Qiunan Xu, Johannes Kroder, Vicky Suess, Horst Borrmann, Chandra Shekhar, Zhaosheng Wang, Chuanying Xi, Wenhong Wang, Walter Schnelle, Steffen Wirth, Yulin Chen, Sebastian T B Goennenwein, and Claudia Felser, “Giant anomalous Hall effect in a ferromagnetic kagome-lattice semimetal,” *Nature Physics* **14**, 1125 – 1131 (2018).
- [11] Linda Ye, Mingu Kang, Junwei Liu, Felix Von Cube, Christina R Wicker, Takehito Suzuki, Chris Jozwiak, Aaron Bostwick, Eli Rotenberg, David C Bell, *et al.*, “Massive dirac fermions in a ferromagnetic kagome metal,” *Nature* **555**, 638–642 (2018).

- [12] Brenden R. Ortiz, Lídia C. Gomes, Jennifer R. Morey, Michal Winiarski, Mitchell Bordelon, John S. Mangum, Iain W. H. Oswald, Jose A. Rodriguez-Rivera, James R. Neilson, Stephen D. Wilson, Elif Ertekin, Tyrel M. McQueen, and Eric S. Toberer, “New kagome prototype materials: discovery of  $KV_3Sb_5$ ,  $RbV_3Sb_5$ , and  $CsV_3Sb_5$ ,” *Physical Review Materials* **3**, 094407 (2019).
- [13] Brenden R. Ortiz, Samuel M. L. Teicher, Yong Hu, Julia L. Zuo, Paul M. Sarte, Emily C. Schueller, A. M. Milinda Abeykoon, Matthew J. Krogstad, Stephan Rosenkranz, Raymond Osborn, Ram Seshadri, Leon Balents, Junfeng He, and Stephen D. Wilson, “ $CsV_3Sb_5$ : A Z2 Topological Kagome Metal with a Superconducting Ground State,” *Physical Review Letters* **125**, 247002 (2020).
- [14] Brenden R Ortiz and PM Sarte, “Superconductivity in the Z2 Kagome metal  $KV_3Sb_5$ ,” arXiv:2012.09097 (2020).
- [15] Shuo-Ying Yang, Yaojia Wang, Brenden R. Ortiz, Defa Liu, Jacob Gayles, Elena Derunova, Rafael Gonzalez-Hernandez, Libor Šmejkal, Yulin Chen, Stuart S. P. Parkin, Stephen D. Wilson, Eric S. Toberer, Tyrel McQueen, and Mazhar N. Ali, “Giant, unconventional anomalous Hall effect in the metallic frustrated magnet candidate,  $KV_3Sb_5$ ,” *Science Advances* **6**, eabb6003 (2020).
- [16] F H Yu, T Wu, Z Y Wang, B Lei, W Z Zhuo, J J Ying, and X H Chen, “Concurrence of anomalous Hall effect and charge density wave in a superconducting topological kagome metal,” arXiv:2102.10987 (2021).
- [17] Yaojia Wang, Shuoying Yang, Pranava K Sivakumar, Brenden R Ortiz, Samuel M L Teicher, Heng Wu, Abhay K Srivastava, Chirag Garg, Defa Liu, Stuart S P Parkin, Eric S Toberer, Tyrel McQueen, Stephen D Wilson, and Mazhar N Ali, “Proximity-induced spin-triplet superconductivity and edge supercurrent in the topological Kagome metal,  $K_{1-x}V_3Sb_5$ ,” arXiv:2012.05898 (2020).
- [18] C C Zhao, L S Wang, W Xia, Q W Yin, J M Ni, Y Y Huang, C P Tu, Z C Tao, Z J Tu, C S Gong, H C Lei, Y F Guo, X F Yang, and S Y Li, “Nodal superconductivity and superconducting dome in the topological Kagome metal  $CsV_3Sb_5$ ,” arXiv:2102.08356 (2021).
- [19] K Y Chen, N N Wang, Q W Yin, Z J Tu, C S Gong, J P Sun, H C Lei, Y Uwatoko, and J G Cheng, “Double superconducting dome and triple enhancement of  $T_c$  in the kagome superconductor  $CsV_3Sb_5$  under high pressure,” arXiv:2102.09328 (2021).
- [20] Yu-Xiao Jiang, Jia-Xin Yin, M Michael Denner, Nana Shumiya, Brenden R Ortiz, Junyi He, Xiaoxiong Liu, Songtian S Zhang, Guoqing Chang, Ilya Belopolski, Qi Zhang, Md Shafayat Hossain, Tyler A Cochran, Daniel Multer, Maksim Litskevich, Zi-Jia Cheng, Xian P Yang, Zurab Guguchia, Gang Xu, Ziqiang Wang, Titus Neupert, Stephen D Wilson, and M Zahid Hasan, “Discovery of topological charge order in kagome superconductor  $KV_3Sb_5$ ,” arXiv:2012.15709 (2020).
- [21] He Zhao, Hong Li, Brenden R Ortiz, Samuel M L Teicher, Taka Park, Mengxing Ye, Ziqiang Wang, Leon Balents, Stephen D Wilson, and Ilija Zeljkovic, “Cascade of correlated electron states in a kagome superconductor  $CsV_3Sb_5$ ,” arXiv:2103.03118 (2021).
- [22] Zuwei Liang, Xingyuan Hou, Wanru Ma, Fan Zhang, Ping Wu, Zongyuan Zhang, Fanghang Yu, J. J. Ying, Kun Jiang, Lei Shan, Zhenyu Wang, and X. H. Chen, “Three-dimensional charge density wave and robust zero-bias conductance peak inside the superconducting vortex core of a kagome superconductor  $CsV_3Sb_5$ ,” arXiv:2103.04760 (2021).
- [23] H. Chen *et al.*, (2021), to be published.
- [24] John P. Perdew, Kieron Burke, and Matthias Ernzerhof, “Generalized gradient approximation made simple,” *Phys. Rev. Lett.* **77**, 3865 (1996).
- [25] Georg Kresse and Jürgen Furthmüller, “Efficiency of ab-initio total energy calculations for metals and semiconductors using a plane-wave basis set,” *Comput. Mater. Sci.* **6**, 15–50 (1996).
- [26] G. Kresse and J. Furthmüller, “Efficient iterative schemes for ab initio total-energy calculations using a plane-wave basis set,” *Phys. Rev. B* **54**, 11169 (1996).
- [27] P. E. Blöchl, “Projector augmented-wave method,” *Phys. Rev. B* **50**, 17953 (1994).
- [28] Stefan Grimme, Jens Antony, Stephan Ehrlich, and Helge Krieg, “A consistent and accurate ab initio parametrization of density functional dispersion correction (dft-d) for the 94 elements h-pu,” *J. Chem. Phys.* **132**, 154104 (2010).
- [29] Atsushi Togo and Isao Tanaka, “First principles phonon calculations in materials science,” *Scr. Mater.* **108**, 1–5 (2015).
- [30] Eric M Kenney, Brenden R Ortiz, Chennan Wang, Stephen D Wilson, and Michael Graf, “Absence of local moments in the kagome metal  $KV_3Sb_5$  as determined by muon spin spectroscopy,” *Journal of Physics: Condensed Matter* (2021), 10.1088/1361-648x/abe8f9.
- [31] J.A. Wilson, F.J. Di Salvo, and S. Mahajan, “Charge-density waves and superlattices in the metallic layered transition metal dichalcogenides,” *Advances in Physics* **24**, 117–201 (1975).
- [32] Supplemental Materials.
- [33] Rudolf Ernst Peierls, *Quantum theory of solids* (Clarendon Press, 1996).
- [34] W. Kohn, “Image of the fermi surface in the vibration spectrum of a metal,” *Phys. Rev. Lett.* **2**, 393–394 (1959).
- [35] Jun Wen, Andreas Rüegg, C.-C. Joseph Wang, and Gregory A. Fiete, “Interaction-driven topological insulators on the kagome and the decorated honeycomb lattices,” *Phys. Rev. B* **82**, 075125 (2010).
- [36] Shun-Li Yu and Jian-Xin Li, “Chiral superconducting phase and chiral spin-density-wave phase in a Hubbard model on the kagome lattice,” *Physical Review B* **85**, 144402 (2012).
- [37] Maximilian L. Kiesel, Christian Platt, and Ronny Thomale, “Unconventional fermi surface instabilities in the kagome hubbard model,” *Phys. Rev. Lett.* **110**, 126405 (2013).
- [38] Wan-Sheng Wang, Zheng-Zhao Li, Yuan-Yuan Xiang, and Qiang-Hua Wang, “Competing electronic orders on kagome lattices at van hove filling,” *Phys. Rev. B* **87**, 115135 (2013).
- [39] Liang Fu and C. L. Kane, “Topological insulators with inversion symmetry,” *Phys. Rev. B* **76**, 045302 (2007).
- [40] J. Bardeen, L. N. Cooper, and J. R. Schrieffer, “Theory of Superconductivity,” *Phys. Rev.* **108**, 1175–1204 (1957).
- [41] W. L. McMillan, “Transition Temperature of Strongly-Coupled Superconductors,” *Phys. Rev.* **167**, 331–344 (1968).

- [42] Charles K Poole, Horacio A Farach, and Richard J Creswick, “Handbook of superconductivity,” (Elsevier, 1999).
- [43] J. M. An and W. E. Pickett, “Superconductivity of  $\text{MgB}_2$ : Covalent Bonds Driven Metallic,” *Phys. Rev. Lett.* **86**, 4366–4369 (2001).
- [44] Chen Si, Zheng Liu, Wenhui Duan, and Feng Liu, “First-principles calculations on the effect of doping and biaxial tensile strain on electron-phonon coupling in graphene,” *Phys. Rev. Lett.* **111**, 196802 (2013).
- [45] F. S. Khan and P. B. Allen, “Deformation potentials and electron-phonon scattering: Two new theorems,” *Phys. Rev. B* **29**, 3341–3349 (1984).
- [46] Qiangwei Yin, Zhijun Tu, Chunsheng Gong, Yang Fu, Shaohua Yan, and Hechang Lei, “Superconductivity and normal-state properties of kagome metal  $\text{rbv}_3\text{sb}_5$  single crystals,” *Chinese Physics Letters* **38**, 037403 (2021).